Remote Sensing of Environment 115 (2011) 3479–3490

Contents lists available at SciVerse ScienceDirect

Remote Sensing of Environment

journal homepage: www.elsevier.com/locate/rse

Remote estimation of chl-*a* concentration in turbid productive waters — Return to a simple two-band NIR-red model?

Daniela Gurlin, Anatoly A. Gitelson *, Wesley J. Moses [1]

Center for Advanced Land Management Information Technologies (CALMIT), School of Natural Resources, University of Nebraska-Lincoln, Lincoln, NE 68583, USA

ARTICLE INFO

Article history:
Received 6 July 2011
Received in revised form 6 July 2011
Accepted 21 August 2011
Available online 26 September 2011

Keywords:
Remote
Estimation
Chl-*a*
Water
MERIS
MODIS

ABSTRACT

Today the water quality of many inland and coastal waters is compromised by cultural eutrophication in consequence of increased human agricultural and industrial activities. Remote sensing is widely applied to monitor the trophic state of these waters. This study investigates the performance of near infrared-red models for the remote estimation of chlorophyll-*a* concentrations in turbid productive waters and evaluates several near infrared-red models developed within the last 34 years. Three models were calibrated for a dataset with chlorophyll-*a* concentrations from 0 to 100 mg m^{-3} and validated for independent and statistically different datasets with chlorophyll-*a* concentrations from 0 to 100 mg m^{-3} and 0 to 25 mg m^{-3} for the spectral bands of the MEdium Resolution Imaging Spectrometer (MERIS) and MODerate resolution Imaging Spectroradiometer (MODIS). The MERIS two-band model estimated chlorophyll-*a* concentrations slightly more accurately than the more complex models, with mean absolute errors of 2.3 mg m^{-3} for chlorophyll-*a* concentrations from 0 to 100 mg m^{-3} and 1.2 mg m^{-3} for chlorophyll-*a* concentrations from 0 to 25 mg m^{-3}. Comparable results from several near infrared-red models with different levels of complexity, calibrated for inland and coastal waters around the world, indicate a high potential for the development of a simple universally applicable near infrared-red algorithm.

1. Introduction

Inland and coastal waters represent complex ecosystems and provide a multitude of ecosystem services (Costanza et al., 1997) to human populations. Due to the essential nature of these services for human welfare, the sustainable management of these ecosystems is an issue of environmental and political concern, and the development of new strategies for the sustainable management of inland and coastal waters might prevent costly measures for the rehabilitation, treatment, and development of new water supplies in the future.

Remote sensing is widely applied to monitor the trophic state of inland and coastal waters (e.g., Kallio et al., 2001; Koponen et al., 2002, 2007; Strömbeck & Pierson, 2001; Thiemann & Kaufmann, 2002) and provides important information for the development of new strategies for the sustainable management of these ecosystems. The concentration of chlorophyll-*a* (chl-*a*), a pigment found in every phytoplankton species, is a measure of the productivity of waters and one of the standard water quality parameters for the evaluation of the trophic state of inland and coastal waters (Baban, 1996; Carlson, 1977; Lillesand et al., 1983). The estimation of chl-*a* concentrations from remotely sensed data requires the development of algorithms with a maximal sensitivity to the concentration of chl-*a* and a minimal sensitivity to the concentrations of the rest of the constituents present in the water.

Many researchers initially concentrated on the interpretation of remotely sensed ocean color and the development of algorithms for oceanic Case I waters (e.g., Gordon & Morel, 1983). In typical Case I waters, the reflectance is influenced by absorption and scattering by phytoplankton particles, the associated debris from grazing by zooplankton and natural decay, and colored dissolved organic matter (CDOM) released from the debris (Bricaud et al., 1981; Gordon & Morel, 1983; Morel & Prieur, 1977). Case I waters comprise the open ocean and are found in coastal areas without a continental shelf and input of terrigenous particles, and in some upwelling regions (Gordon & Morel, 1983). Contrary to Case I waters, the reflectance in Case II waters is controlled by inorganic particles and the contribution of phytoplankton pigments to total absorption in ideal Case II waters is minimal (Morel & Prieur, 1977). Reflectance of Case II waters is influenced by re-suspended sediments, terrigenous particles and CDOM, and particulate and dissolved materials of anthropogenic origin (Gordon & Morel, 1983). Inland and coastal waters are optically complex and may combine the optical properties of Case I and Case II waters. Reflectance of these waters is controlled by the combined effects of absorption and scattering by phytoplankton particles, inorganic and organic particles, and CDOM.

* Corresponding author. Tel.: +1 402 472 8386; fax: +1 402 472 2946.
E-mail addresses: dgurlin12@huskers.unl.edu (D. Gurlin), agitelson2@unl.edu (A.A. Gitelson), wesley.moses.ctr.in@nrl.navy.mil (W.J. Moses).
[1] Present address: Research Associate, The National Research Council at the Naval Research Laboratory, Washington, DC 20375, USA.

0034-4257/$ – see front matter © 2011 Elsevier Inc. All rights reserved.
doi:10.1016/j.rse.2011.08.011

Standard algorithms for the estimation of chl-*a* concentrations in the open ocean rely on reflectances in the blue and green spectral regions (O'Reilly et al., 2000). In inland and coastal waters, the reflectance in these spectral regions is highly affected by the presence of particles and CDOM and the combined absorption by phytoplankton pigments, particles, and CDOM in the blue and green spectral regions is seldom correlated with the concentration of phytoplankton particles. Consequently, the algorithms typically applied for the remote estimation of chl-*a* concentrations in oceanic waters are ineffective in many inland and coastal waters and researchers have directed their efforts toward the development of different algorithms for the remote estimation of chl-*a* concentrations in these waters (e.g., Dekker et al., 1991; Gitelson et al., 1985; Gitelson, 1992; Gons, 1999; Gons et al., 2000; Gons et al., 2002; Gons et al., 2008; Gower, 1980; Gower et al., 1999; Kallio et al., 2001; Neville & Gower, 1977; Strömbeck & Pierson, 2001; Vasilkov & Kopelevich, 1982).

Studies of the optical properties of inland and coastal waters revealed the potential of the red and near infrared (NIR) spectral regions, where the reflectance is less affected by the presence of particles and CDOM, for the remote estimation of chl-*a* concentrations and initiated the development of algorithms based on these spectral regions. These algorithms take advantage of several spectral features related to chl-*a* in the red and NIR spectral regions.

Some algorithms are based on the quantification of the reflectance (ρ) peak at 685 nm caused by solar-induced chl-*a* fluorescence (Neville & Gower, 1977). Gower (1980) suggested using the peak magnitude at 685 nm above a baseline from 650 to 730 nm, the fluorescence line height (FLH), for the estimation of chl-*a* concentrations. Today the estimation of chl-*a* concentrations through the FLH is typically applied in coastal waters and parts of the open ocean (Gower & King, 2007; Ryan et al., 2009). Disadvantages of the FLH include its sensitivity to the natural variability of the chl-*a* specific absorption coefficient of phytoplankton, $a^*_\varphi(\lambda)$, the re-absorption of fluoresced light by chl-*a*, and the natural variability of the quantum yield of chl-*a* fluorescence (Babin et al., 1996).

Many algorithms for the remote estimation of chl-*a* concentrations in inland and coastal waters are based on the reflectance peak around 700 nm, caused by a minimum in the combined absorption by phytoplankton pigments and water (Gitelson, 1992; Han & Rundquist, 1997; Vasilkov & Kopelevich, 1982), and the reflectance trough at 675 nm. The latter is related to the chl-*a* absorption maximum in the red region. Some algorithms explored the ratio of the reflectance at the peak around 700 nm to the reflectance at the peak around 560 nm, which is related to a minimum in the combined absorption by phytoplankton pigments, particles, and CDOM. Close relationships, with Pearson correlation coefficients (r) of 0.91 to 0.99, were found between $\rho(700)/\rho(560)$ and chl-*a* concentration for the rivers Don and Donec in Russia, the Azov Sea, and Lake Balaton in Hungary (Gitelson et al., 1986). Alternative algorithms included the position and magnitude of the reflectance peak around 700 nm (e.g., Gitelson, 1992; Gitelson & Kondratyev, 1991), the reflectance ratios $\rho(705)/\rho(675)$ and $\rho(705)/\rho(670)$, (e.g., Dekker, 1993; Gitelson et al., 1985; Han & Rundquist, 1997; Mittenzwey et al., 1991, 1992; Quibell, 1991), and some more complex empirical algorithms (e.g., Mittenzwey et al., 1991).

Models for the remote estimation of chl-*a* concentrations are based on a fundamental relationship (Gordon, 1973; Gordon et al., 1975) of remote sensing reflectance, $\rho_{rs}(\lambda)$, and the inherent optical properties of water — the absorption coefficient, $a(\lambda)$, and the backscattering coefficient, $b_b(\lambda)$:

$$\rho_{rs}(\lambda) = \frac{f(\lambda)}{Q(\lambda)} \frac{b_b(\lambda)}{a(\lambda)+b_b(\lambda)} \tag{1}$$

where $f(\lambda)$ describes the sensitivity of the reflectance to variations in the solar zenith angle (Morel & Gentili, 1991) and $Q(\lambda)$ expresses the bidirectional properties of the reflectance (Morel & Gentili, 1993). Gons (1999) reformulated the ratio $\rho(705)/\rho(675)$ in terms of $a(\lambda)$ and $b_b(\lambda)$ for subsurface irradiance reflectance spectra and partitioned $a(\lambda)$ into the absorption coefficients of phytoplankton, $a_\varphi(\lambda)$, non-algal particles, $a_{NAP}(\lambda)$, CDOM, $a_{CDOM}(\lambda)$, and water, $a_w(\lambda)$, to develop a semi-analytical model in the form:

$$[\text{Chl}-a] = \frac{\frac{\rho(704)}{\rho(672)}(a_w(704)+b_b) - a_w(672) - b_b{}^p}{a^*_\varphi(672)} \tag{2}$$

where $a^*_\varphi(672)$ is the chl-*a* specific absorption coefficient of phytoplankton at 672 nm and p was introduced to improve the fit of the model. This model is based on several simplifications: (a) the absorption at 672 nm is controlled by chl-*a* and water and is minimally affected by the rest of the constituents, (b) the absorption by pigments, particles, and CDOM at 704 nm is insignificant compared to the absorption by water, and (c) b_b is wavelength independent and can be derived from the reflectance in the NIR region. The coefficients for $a^*_\varphi(672)$ and p were retrieved through regression for datasets from several inland waters.

Dall'Olmo et al. (2003) applied a conceptual model, originally developed for the estimation of the total foliar chl-*a* content in terrestrial vegetation (Gitelson et al., 2003), to turbid productive waters:

$$\left[\text{Chl}-a\right] \propto \left[\rho_{rs}^{-1}(\lambda_1) - \rho_{rs}^{-1}(\lambda_2)\right] \times \rho_{rs}(\lambda_3) \tag{3}$$

where $\rho_{rs}^{-1}(\lambda_1)$ is considered maximally sensitive to absorption by chl-*a*, even though it is still affected by absorption and scattering by the rest of the constituents, and $\rho_{rs}^{-1}(\lambda_2)$ is minimally sensitive to absorption by chl-*a*. If the sensitivities of $\rho_{rs}^{-1}(\lambda_2)$ and $\rho_{rs}^{-1}(\lambda_1)$ to the presence of NAP and CDOM are comparable, it is possible to remove the effects of the absorption by these constituents through the subtraction of $\rho_{rs}^{-1}(\lambda_2)$ from $\rho_{rs}^{-1}(\lambda_1)$. $\rho_{rs}(\lambda_3)$ is minimally sensitive to absorption by chl-*a*, NAP, and CDOM and representative of $b_b(\lambda)$. The multiplication of $[\rho_{rs}^{-1}(\lambda_1) - \rho_{rs}^{-1}(\lambda_2)]$ with $\rho_{rs}(\lambda_3)$ should remove the effects of the variability in $b_b(\lambda)$ on the chl-*a* estimation. The optimal wavelengths for the estimation of chl-*a* concentrations from 2 to 180 mg m^{-3} were identified at $\lambda_1 = 670$ nm, $\lambda_2 = 710$ nm, and $\lambda_3 = 740$ nm (Dall'Olmo & Gitelson, 2005). The three-band model relies, similar to Gons' model (Gons, 1999), on a wavelength independent b_b in the spectral range from λ_1 to λ_3. For waters without high concentrations of NAP and CDOM it is possible to disregard the subtraction of $\rho_s^{-1}(\lambda_2)$ and this special case corresponds to a two-band model developed by Stumpf and Tyler (1988):

$$\left[\text{Chl}-a\right] \propto \rho_{rs}^{-1}(\lambda_1) \times \rho_{rs}(\lambda_3) \tag{4}$$

which is fundamentally different from the widely applied reflectance ratio (Gitelson et al., 1985; Gitelson, 1992; Mittenzwey et al., 1991):

$$\left[\text{Chl}-a\right] \propto \rho_{rs}^{-1}(\lambda_1) \times \rho_{rs}(\lambda_2) \tag{5}$$

where $\rho_{rs}^{-1}(\lambda_1)$ is the reflectance around the chl-*a* absorption maximum in the red region at 675 nm and $\rho_{rs}^{-1}(\lambda_2)$ represents the reflectance peak around 705 nm.

Even though the three-band (Eq. 3) and two-band models (Eqs. 4 and 5) are potentially susceptible to the natural variability of the chl-*a* specific absorption coefficient of phytoplankton and the quantum yield of chl-*a* fluorescence, they were successfully applied for the remote estimation of chl-*a* concentrations with field spectrometers (Gitelson et al., 2008, 2011; Yacobi et al., 2011), satellites (Moses et al., 2009), and modeled reflectance spectra (Gilerson et al., 2010).

The objective of this study was to investigate the performance of NIR-red models for the estimation of chl-*a* concentrations in turbid productive waters. This study shows (1) the importance of the red and NIR

spectral regions for the remote estimation of chl-*a* concentrations in turbid productive waters, (2) the application of three NIR-red models, calibrated and validated for the spectral bands of the MERIS and MODIS satellite sensors, for the remote estimation of low-to-moderate chl-*a* concentrations, typical for many inland and coastal waters, for independent and statistically different datasets, and (3) the potential of a simple two-band NIR-red algorithm for the MERIS satellite sensor to accurately estimate chl-*a* concentrations in comparison with several more complex recently published NIR-red algorithms.

2. Methods

2.1. Field measurements

Field data were collected at 89 stations in summer and autumn 2008 and at 63 stations in spring and summer 2009 in the Fremont Lakes State Recreation Area in Nebraska, USA, which comprises of 20 sandpit lakes. The highly variable bio-physical and bio-optical conditions found in the Fremont Lakes are typical for many inland and coastal waters and make these lakes ideal for the development of algorithms for the remote estimation of chl-*a* concentrations in turbid productive waters.

The field measurements included a standard set of water quality parameters and hyperspectral reflectance measurements. Surface water samples for the laboratory analysis of the chl-*a* concentrations, suspended solids, and the absorption coefficients of total particulates, NAP, phytoplankton, and CDOM were collected at a depth of 0.5 m and stored in a dark and cool container for subsequent filtration through Whatman GF/F filters.

Volume scattering coefficients, $\beta(\theta, \lambda)$, were measured in 2009 with a customized ECO Triplet sensor (WET Labs, Inc.) and corrected for salinity, $a_w(\lambda)$, $a_p(\lambda)$, and $a_{CDOM}(\lambda)$. The values for $a_w(\lambda)$ were taken from Mueller (2003) and the values for $a_p(\lambda)$ and $a_{CDOM}(\lambda)$ from the laboratory measurements. The volume scattering of particles, $\beta_p(117°, \lambda)$, and volume scattering of water, $\beta_w(117°, \lambda)$ were derived from the corrected volume scattering coefficients, $\beta(117°, \lambda)$, to calculate the particulate backscattering coefficients, $b_{bp}(\lambda)$. The backscattering coefficients, $b_b(\lambda)$, were calculated from the sum of $b_{bp}(\lambda)$ and the backscattering coefficients of pure water, $b_{bw}(\lambda)$, (WET Labs, Inc., 2008). Additional field measurements included water transparency, measured with a standard Secchi disk, and turbidity, measured with a HACH® 2100 portable turbidimeter.

Hyperspectral reflectance measurements were collected with two inter-calibrated Ocean Optics® USB2000 spectrometers in areas of optically deep water in the spectral range from 400 to 900 nm with a spectral resolution of ~0.3 nm. One of the spectrometers was connected to a 25° field-of-view optical fiber. The optical fiber was taped to a 2-m long, hand-held dark blue pole and the tip of the fiber was kept just beneath the water surface to measure the below-surface upwelling radiance, $L_u(\lambda)$, at nadir on the sun-lit side of the boat. The second spectrometer was connected to an optical fiber fitted with a cosine collector to create a 180° field-of-view. The optical fiber was mounted on a mast at the highest possible point on the boat to measure the incident irradiance, $E_d(\lambda)$, at zenith concurrently with the upwelling radiance. The measurements were collected from 10 a.m. to 2 p.m. with widely variable solar zenith angles. Inter-calibration of the instruments, to account for potential differences in their transfer functions, was achieved through synchronized measurements of the upwelling radiance, $L_{ref}(\lambda)$, from a white Spectralon® reflectance standard (Labsphere, Inc.), and the irradiance incident on the standard, $E_{ref}(\lambda)$. The remote sensing reflectance was computed by:

$$\rho_{rs}(\lambda) = \frac{L_u(\lambda)}{E_d(\lambda)} \times \frac{E_{ref}(\lambda)}{L_{ref}(\lambda)} \times 100 \times \frac{\rho_{ref}(\lambda)}{\pi} \times \frac{t}{n^2} \times F(\lambda) \quad (6)$$

where $\rho_{ref}(\lambda)$ is the irradiance reflectance of the Spectralon® reflectance standard, π is introduced to transform the irradiance reflectance $\rho_{ref}(\lambda)$ into a radiance reflectance, t is the water-to-air transmittance, n is the refractive index of water relative to air ($n = 1.33$ at 20 °C), and $F(\lambda)$ is the spectral immersion factor (Ohde & Siegel, 2003). The spectra were processed in real time with the software CDAP, developed at CALMIT, University of Nebraska-Lincoln, and the median of at least six spectra collected at each station was considered representative for the station.

2.2. Laboratory measurements

Chl-*a* was extracted in 99.5% ethanol at a temperature of 78 °C in subdued light conditions in a laboratory at the University of Nebraska-Lincoln (Nusch, 1980). The samples were centrifuged for 5 min after an extraction time of 4 h and chl-*a* concentrations were measured fluorometrically with a Turner 10-AU-005 CE fluorometer (Welschmeyer, 1994). The fluorometer was calibrated every 3 months with a 100 mg m^{-3} chl-*a* standard from *Anacystis nidulans* (C6144-1MG from Sigma Aldrich). Therefore the chl-*a* was dissolved in 1 L 99.5% ethanol and the concentration of the standard was measured spectrophotometrically (Ritchie, 2008). Standard curves to study the linearity of the single point calibration of the fluorometer for chl-*a* concentrations from 0 to 200 mg m^{-3} were created at the time of calibration and included a series of 10 dilutions. The concentrations of total suspended solids (TSS), inorganic suspended solids (ISS), and organic suspended solids (OSS) were measured gravimetrically (Eaton et al., 2005).

The absorption coefficients were analyzed with the quantitative filter technique (Mitchell et al., 2003). The measurements of the optical density of the particles retained on the filters were made shortly after the filtration of the water samples with a Cary 100 spectrophotometer in the range from 400 to 800 nm. The signal from a Milli-Q saturated reference filter was subtracted automatically and $a_p(\lambda)$ was calculated by:

$$a_p(\lambda) = \frac{\ln(10)}{\frac{V}{A}} \left[0.3893 \times \left[OD_{fp}(\lambda) - OD_{null} \right] + 0.4340 \times \left[OD_{fp}(\lambda) - OD_{null} \right]^2 \right] \quad (7)$$

where $OD_{fp}(\lambda)$ is the optical density of the sample, $OD_{null}(\lambda)$ is the average optical density of the sample from 780 to 800 nm required for the null point correction of the measurements, V is the volume of water filtered in m^3, and A is the area of the filter in m^2. The quadratic function for the pathlength amplification correction (Cleveland & Weidemann, 1993) included in the equation was derived by Dall'Olmo (2006) for water samples from lakes and reservoirs in Nebraska and laboratory cultures of *Microcystis* and *Synechoccus*. The effects of the absorption by pigments were removed after Ferrari and Tassan (1999) and $a_{NAP}(\lambda)$ was measured similarly to $a_p(\lambda)$ after a 20 minute reaction time. The subtraction of $a_{NAP}(\lambda)$ from $a_p(\lambda)$ resulted in $a_\varphi(\lambda)$.

The filtrates from the TSS measurements were filtered through 0.2 µm Whatman nylon membranes for the analysis of $a_{CDOM}(\lambda)$. The absorption coefficients were measured shortly after the filtration of the samples with the Cary 100 spectrophotometer in the range from 200 to 800 nm and the signal from a Milli-Q water reference sample was subtracted automatically. The samples were kept at a constant temperature to minimize a temperature related absorption feature found around 750 nm (Pegau et al., 1997). The absorption coefficients were calculated as:

$$a_{CDOM}(\lambda) = \frac{\ln(10)}{l} \left[OD_s(\lambda) - OD_{null} \right] \quad (8)$$

where $OD_s(\lambda)$ is the optical density of the sample, $OD_{null}(\lambda)$ is the average optical density of the sample from 780 to 800 nm for the null point correction, and l is the pathlength of the cuvette in m. More

Table 1
Descriptive statistics of the water quality parameters measured in 2008.

	N	Min	Max	Median	Mean	Standard deviation	CV (%)
Chl-*a* (mg m^{-3})	89	2.27	200.81	27.44	33.54	29.44	87.8
Secchi disk depth (m^{-1})	89	0.51	4.20	0.98	1.21	0.70	57.9
Turbidity (NTU)	89	1.51	19.20	6.79	7.59	4.39	57.8
TSS (g m^{-3})	89	1.19	15.00	6.80	7.30	3.26	44.6
ISS (g m^{-3})	87	0.15	5.85	0.80	1.11	0.95	85.7
OSS (g m^{-3})	87	0.81	12.80	6.00	6.26	2.97	47.5
a_p (675) (m^{-1})	80	0.0470	4.4867	0.4996	0.5915	0.5683	96.1
a_{NAP} (675) (m^{-1})	80	0.0031	0.2940	0.0595	0.0725	0.0554	76.4
a_φ (675) (m^{-1})	80	0.0440	4.4051	0.4017	0.5190	0.5623	108.3
a^*_φ(675) (m^2 mg^{-1})	80	0.0059	0.0285	0.0143	0.0156	0.0052	33.3
a_{CDOM} (440) (m^{-1})	80	0.4553	1.4525	0.8946	0.8806	0.2468	28.0
a_{CDOM} (675) (m^{-1})	80	0.0069	0.0333	0.0153	0.0158	0.0057	36.1
S_{CDOM} (nm^{-1})	80	0.0156	0.0185	0.0173	0.0172	0.0006	3.6

Chl-*a* — chlorophyll-*a* concentration, TSS — concentration of *t*otal *s*uspended *s*olids, ISS — concentration of *i*norganic *s*uspended *s*olids, OSS — concentration of *o*rganic *s*uspended *s*olids, $a_p(675)$ — total particulate absorption coefficient at 675 nm, $a_{NAP}(675)$ — absorption coefficient of non-algal particles at 675 nm, $a_\varphi(675)$ — absorption coefficient of phytoplankton at 675 nm, $a^*_\varphi(675)$ — chl-*a* specific absorption coefficient of phytoplankton at 675 nm, $a_{CDOM}(440)$ and $a_{CDOM}(675)$ — absorption coefficients of CDOM at 440 and 675 nm calculated after Bricaud et al. (1981), N — number of samples, and CV — coefficient of variation.

details of the steps in the laboratory analysis of the water samples are presented in Gitelson et al. (2011).

2.3. Model calibration and validation

Three NIR-red models were calibrated and validated for the spectral bands of the MERIS (Eqs. 3 and 5) and MODIS (Eq. 4) satellite sensors to estimate chl-*a* concentrations in the Fremont Lakes. The models were calibrated for the dataset collected in summer and fall 2008 and validated for the dataset collected in spring and summer 2009. The accuracy of the models was assessed through the mean absolute error (MAE), the root mean squared error (RMSE), and the mean normalized absolute error (MNAE). To compare the absolute estimation errors of these algorithms with the errors from several recently published NIR-red algorithms, a one-way analysis of variance (ANOVA), followed by Tukey's honestly significant difference multiple comparison procedure (Tukey's HSD), was performed in PASW® Statistics 18.0 (SPSS, Inc.).

3. Results and discussion

3.1. Bio-physical and bio-optical water quality parameters

The descriptive statistics of the water quality parameters measured in the Fremont Lakes in 2008 and 2009 (Tables 1 and 2) indicate optical conditions typical for turbid productive inland and coastal waters (e.g., Kallio et al., 2001; Koponen et al., 2002, 2007). Chl-*a* concentrations ranged from 2.3 to 200.8 mg m^{-3} in 2008 and from 4.0 to 196.4 mg m^{-3} in 2009. The distributions of the chl-*a* concentrations measured in 2008 and 2009 were significantly different from normal distributions (Shapiro–Wilk test, $p<0.01$) and skewed toward lower chl-*a* concentrations with only 14 stations with chl-*a* concentrations of more than 50 mg m^{-3} in 2008 and 9 stations in 2009.

TSS concentrations ranged from 1.2 to 15.0 g m^{-3} in 2008 and from 1.3 to 22.9 g m^{-3} in 2009. ISS concentrations ranged from 0.1 to 5.8 g m^{-3} in 2008 and from 0.1 to 6.2 g m^{-3} in 2009. The contribution of ISS to TSS ranged widely from only 2.8 to 57.8% in 2008 and 2.4 to 61.1% in 2009. The median contribution of ISS to TSS was 12.2% in 2008 and 19.2% in 2009.

The water quality parameters measured in 2008 and 2009 (Tables 1 and 2) were statistically significantly different (Mann–Whitney *U* test, $p\leq0.05$), with the exception of Secchi disk depth ($p=0.16$), TSS ($p=0.06$), and ISS ($p=0.60$).

The spectra of $a_p(\lambda)$, $a_{NAP}(\lambda)$, $a_\varphi(\lambda)$, and $a_{CDOM}(\lambda)$ showed a high variability in 2008 and 2009 (Fig. 1). The particulate absorption coefficient, $a_p(440)$, was typical for inland and coastal waters and ranged from 0.292 to 6.860 m^{-1} in 2008 and from 0.287 to 7.482 m^{-1} in 2009 with coefficients of variation of 56.2% in 2008 and 87.7% in 2009. Spearman correlation coefficients (r_s) indicated a close relationship ($p<0.01$) with the chl-*a* ($r_s=0.82$), TSS ($r_s=0.78$), OSS ($r_s=0.75$), and ISS ($r_s=0.40$) concentrations in 2008. The absorption coefficient of phytoplankton, $a_\varphi(440)$, ranged from 0.061 to 5.598 m^{-1} and was highly correlated with the chl-*a* concentration ($r_s=0.80$). These relationships were comparable to those in 2009, where the correlations of $a_p(440)$ with chl-*a* ($r_s=0.92$), TSS ($r_s=0.90$), and OSS ($r_s=0.92$) concentrations were even stronger

Table 2
Descriptive statistics of the water quality parameters measured in 2009.

	N	Min	Max	Median	Mean	Standard deviation	CV (%)
Chl-*a* (mg m^{-3})	63	3.97	196.39	16.07	30.03	35.19	117.2
Secchi disk depth (m^{-1})	63	0.39	3.32	1.12	1.37	0.77	56.0
Turbidity (NTU)	63	1.08	23.40	4.73	6.08	5.31	87.4
TSS (g m^{-3})	63	1.32	22.89	5.83	6.67	4.67	70.1
ISS (g m^{-3})	63	0.10	6.22	1.00	1.39	1.40	100.2
OSS (g m^{-3})	63	0.85	17.00	4.50	5.28	3.99	75.6
a_p (675) (m^{-1})	63	0.0650	2.8214	0.2922	0.4764	0.5371	112.7
a_{NAP} (675) (m^{-1})	63	0.0071	0.1131	0.0447	0.0504	0.0270	53.6
a_φ (675) (m^{-1})	63	0.0411	2.7204	0.2282	0.4261	0.5220	122.5
a^*_φ(675) (m^2 mg^{-1})	63	0.0091	0.0203	0.0136	0.0137	0.0021	15.3
a_{CDOM} (440) (m^{-1})	63	0.3530	1.3489	0.6475	0.6852	0.2203	32.1
a_{CDOM} (675) (m^{-1})	63	0.0027	0.0234	0.0086	0.0100	0.0047	47.0
S_{CDOM} (nm^{-1})	63	0.0165	0.0210	0.0182	0.0182	0.0009	5.2
b_{bp}(570) (m^{-1})	44	0.0237	0.1740	0.0855	0.0822	0.0397	48.3
b_{bp}(660) (m^{-1})	44	0.0155	0.0944	0.0562	0.0526	0.0248	47.2
b_{bp}(740) (m^{-1})	44	0.0144	0.0900	0.0601	0.0559	0.0248	44.4

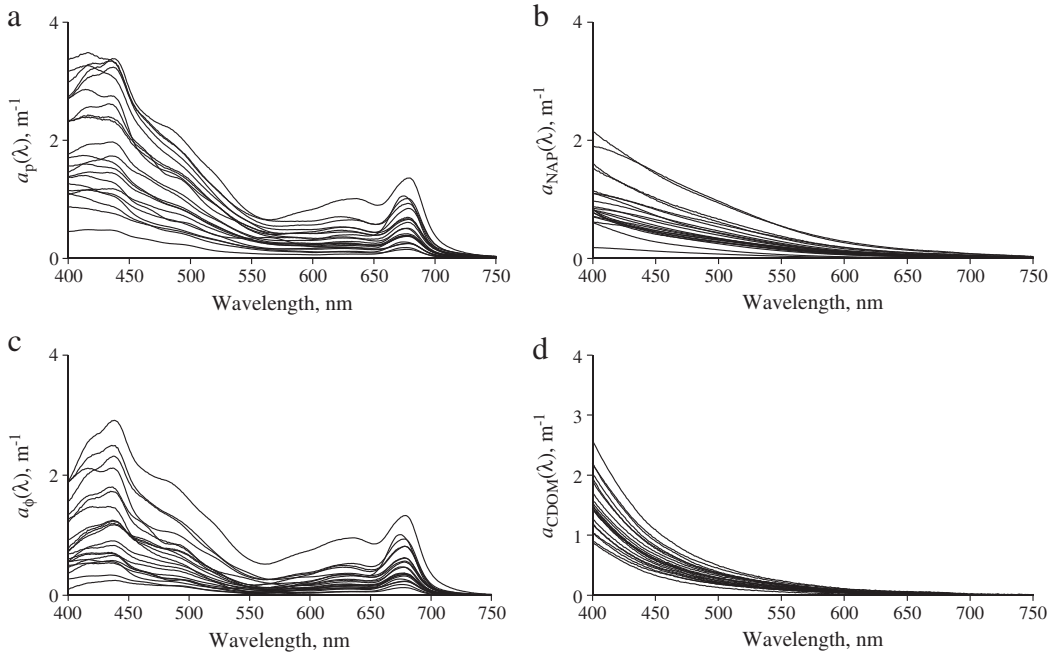

Fig. 1. Representative spectra of the absorption coefficients of total particulates (a), non-algal particles (b), phytoplankton (c), and CDOM (d) for 21 stations with chl-*a* concentrations from 2.3 to 132.4 mg m^{-3}.

due to relatively low concentrations of ISS in spring 2009, and $a_\varphi(440)$ was highly correlated with the chl-*a* concentration ($r_s = 0.96$). Even though $a_p(440)$ was related to the chl-*a* concentration in 2008 and 2009, it was still influenced by $a_{NAP}(440)$. The contribution of $a_\varphi(440)$ to total particulate absorption ranged widely from 9.6 to 93.4% in 2008 and from 8.0 to 91.1% in 2009. Some of the spectra of $a_{NAP}(\lambda)$ showed a deviation from the typical exponential shape (Fig. 1) comparable to spectra taken at the Baltic Sea (Babin et al., 2003).

In the red spectral region, mainly phytoplankton pigments contributed to total particulate absorption and the median contribution of $a_\varphi(675)$ to $a_p(675)$ was 87.6% in 2008 and 83.9% in 2009. Consequently, $a_\varphi(675)$ was highly correlated ($p<0.01$) with the concentration of chl-*a* in 2008 ($r_s = 0.87$) and 2009 ($r_s = 0.98$). The relatively small $a_{NAP}(675)$ and $a_{CDOM}(675)$ compared to $a_\varphi(675)$, in the waters studied (Tables 1 and 2), confirm the importance of the red spectral region for the development of algorithms for the remote estimation of chl-*a* concentrations in inland and coastal waters.

The spectra of the chl-*a* specific absorption coefficient of phytoplankton, $a^*_\varphi(\lambda)$, showed a high variability and indicate seasonal differences in the physiological status of the phytoplankton and species composition in the Fremont Lakes. $a^*_\varphi(440)$ and $a^*_\varphi(675)$ were only slightly correlated with the chl-*a* concentration and the correlation decreased with an increase in chl-*a* concentration ($r_s = -0.27$ for $a^*_\varphi(440)$ and $r_s = -0.39$ for $a^*_\varphi(675)$, $p<0.05$) in 2008 (Fig. 2). In 2009 the relationship was less variable than in 2008 with a slight increase of $a^*_\varphi(440)$ and $a^*_\varphi(675)$ with an increase in chl-*a* concentration ($r_s = 0.68$ for $a^*_\varphi(440)$, $p<0.05$ and $r_s = 0.24$ for $a^*_\varphi(675)$, $p = 0.06$). The differences of the relationships $a^*_\varphi(\lambda)$ versus chl-*a* concentration in 2008 and 2009 may be related to seasonal differences in the species composition of the phytoplankton community and, therefore, differences in the composition of phytoplankton pigments and pigment package effects (Bricaud et al., 1995).

The spectral slope of the absorption coefficient of CDOM, S_{CDOM}, ranged from 0.0156 to 0.0185 nm^{-1} in 2008 and from 0.0165 to 0.0210 nm^{-1} in 2009 and is typical for inland (e.g., Binding et al., 2008) and coastal (e.g., Babin et al., 2003) waters. The S_{CDOM} values were normally distributed and averaged 0.0172 nm^{-1} in 2008 and 0.0182 nm^{-1} in 2009. Small seasonal differences were found in 2008, where the average S_{CDOM} was 0.0173 nm^{-1} in the summer and decreased slightly to 0.0171 nm^{-1} in autumn, compared to 2009, where the average S_{CDOM} reached its maximum of 0.0185 nm^{-1} in spring and decreased to 0.0175 nm^{-1} in summer. The conspicuous intra-annual differences found in a_{CDOM} (440) and S_{CDOM} might indicate differences in the molecular weight of humus (Carder et al., 1989; Hayase & Tsubota, 1985) caused by seasonal differences in the input and decomposition of organic materials and different sources of CDOM.

The spectra of the backscattering coefficients, $b_b(\lambda)$, were comparable to spectra of moderately turbid inland and coastal waters (e.g., Kutser et al., 2009). The backscattering coefficients ranged from 0.024 to 0.174 m^{-1} at 570 nm, from 0.016 to 0.095 m^{-1} at 660 nm and from 0.015 to 0.090 m^{-1} at 740 nm. They decreased from 660 to 740 nm for 10 out of 44 stations and, even though the differences in $b_b(660)$ and $b_b(740)$ were statistically insignificant (Mann–Whitney *U* test, $p = 0.48$), the reliability of models for the remote estimation of chl-*a* concentrations, in which a wavelength independent $b_b(\lambda)$ in the range from 660 through 750 nm is assumed, is potentially affected.

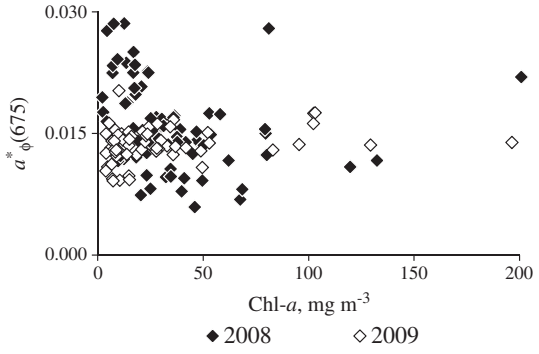

Fig. 2. Chl-*a* specific absorption coefficient of phytoplankton at 675 nm, $a^*_\varphi(675)$, shown versus chl-*a* concentration for the Fremont Lakes 2008 and 2009 datasets. Even though $a^*_\varphi(675)$ appears comparable in 2008 and 2009, a negative correlation of chl-*a* concentration and $a^*_\varphi(675)$ was found in 2008, while no statistically significant correlation was found in 2009.

The particulate backscattering coefficients, $b_{bp}(\lambda)$, were closely related to the OSS concentration and minimally related to the ISS concentration. The increase in the correlation coefficient of the relationship $b_{bp}(\lambda)$ vs. TSS from $r_s = 0.80$ for $b_{bp}(570)$ to $r_s = 0.84$ for $b_{bp}(740)$ shows an increased effect of the particle concentration on $b_{bp}(\lambda)$ at longer wavelengths.

3.2. Reflectance

The reflectance spectra collected in 2008 and 2009 (Fig. 3) showed a high variability in the visible and NIR spectral regions and are comparable to spectra collected around the world (e.g., Yacobi et al., 2011; Yang et al., 2010). In the blue spectral region, the reflectance was low and without any distinctive spectral features due to combined absorption by phytoplankton pigments, NAP, and CDOM. The trough related to the chl-*a* absorption maximum, typically found at 440 nm in oceanic waters (Bidigare et al., 1990), was concealed by the absorption by NAP and CDOM for many stations with chl-*a* concentrations from 0 to 50 mg m^{-3}. The reflectance increased in the green region and reached a maximum around 570 nm, where the absorption by phytoplankton pigments was minimal and reflectance was mainly affected by NAP and CDOM. The reflectance in the red and NIR regions was characterized by a trough at 675 nm, which corresponds to the red chl-*a* absorption maximum (Bidigare et al., 1990), and a peak around 700 nm, related to a minimum in the combined absorption by phytoplankton pigments and water (Gitelson, 1992; Vasilkov & Kopelevich, 1982). The magnitude of the reflectance was highly variable and the coefficients of variation in the different spectral regions ranged from 42.1 to 81.9% in 2008 and 31.1 to 86.2% in 2009 (Fig. 3).

3.3. Blue-green vs. red spectral region

Maximum band ratios (O'Reilly et al., 2000) for the remote estimation of chl-*a* concentrations in oceanic waters in the form of the MERIS OC4E and MODIS OC3M-551 algorithms rely on band combinations in the blue and green spectral regions. These spectral regions

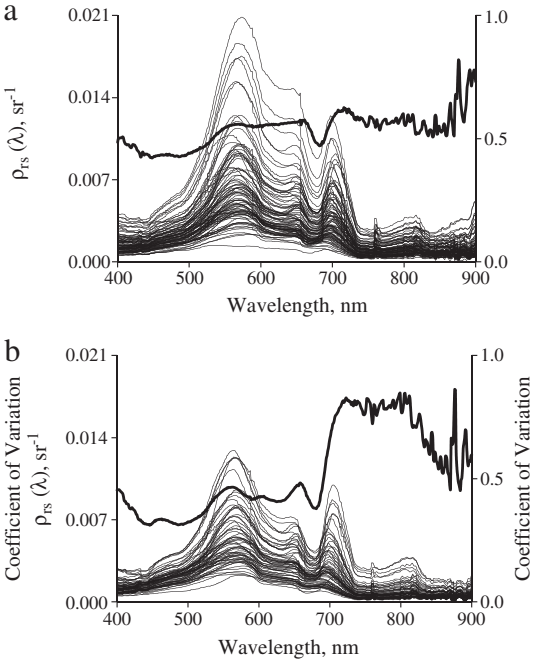

Fig. 3. Remote sensing reflectance spectra for the waters sampled in 2008 (a) and 2009 (b). The thick line represents the coefficient of variation of the reflectance.

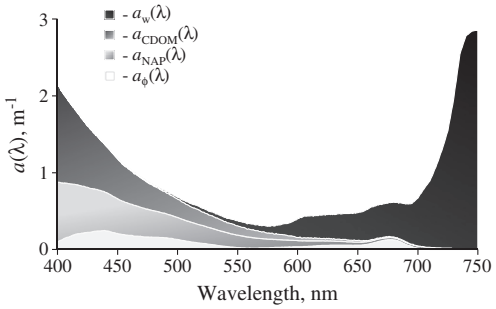

Fig. 4. Spectra of the absorption coefficients of phytoplankton, non-algal particles, CDOM, and water for a lake with a chl-*a* concentration of 4.6 mg m^{-3} and TSS concentration of 3.5 g m^{-3} (values for the absorption coefficient of water taken from Mueller, 2003).

are highly affected by the absorption by NAP and CDOM in inland and coastal waters.

This is exemplified by spectra of $a_\varphi(\lambda)$, $a_{NAP}(\lambda)$, $a_{CDOM}(\lambda)$, and $a_w(\lambda)$ for a station in a lake with a chl-*a* concentration of 4.6 mg m^{-3} and TSS concentration of 3.5 g m^{-3} (Fig. 4). In the blue region, the contribution of $a_\varphi(442.5)$ to total absorption was only 18.0% compared to contributions of 36.8% by $a_{NAP}(442.5)$ and 44.5% by $a_{CDOM}(442.5)$. The contribution of $a_w(442.5)$ to total absorption was minimal. These relationships changed only slightly at 490 and 510 nm. In the green region, the contribution of $a_\varphi(560)$ to total absorption decreased to 6.2%, the combined contribution by $a_{NAP}(560)$ and $a_{CDOM}(560)$ was 72.5%, and the contribution by $a_w(560)$ increased to 21.3%. The total absorption coefficient was closely related to the absorption by NAP and CDOM for wavelengths from 400 to 565 nm and decreased exponentially ($R^2 = 0.9995$) toward longer wavelengths.

Thus, in the waters studied, the MERIS OC4E algorithm, based on the maximal ratio of $\rho(442.5)/\rho(560)$, $\rho(490)/\rho(560)$, and $\rho(510)/\rho(560)$ and the MODIS OC3M-551 algorithm, based on the maximal ratio of $\rho(443)/\rho(551)$ and $\rho(489)/\rho(551)$ were unable to accurately estimate chl-*a* concentrations. The normalized absolute error (NAE) exceeded 186.6% when the MERIS OC4E algorithm was applied for the station shown (Fig. 4) and the MNAE was still 34.4% when the same algorithm was applied for the Fremont Lakes 2009 dataset with chl-*a* concentrations from 0 to 100 mg m^{-3} (Fig. 5).

In contrast to the blue and green regions, the contributions of $a_{NAP}(675)$ and $a_{CDOM}(675)$ to total absorption were only 2.0 and 4.5%, respectively, in the red region (Fig. 4). The contribution of $a_\varphi(675)$ increased to 20.9% and the main contribution came from $a_w(675)$ with 72.6%. The minimal absorption by NAP and CDOM and distinctive absorption features of chl-*a*, with maximal absorption around 675 nm and minimal combined absorption by water and phytoplankton pigments around 700 nm, in addition to the well-known absorption coefficient of water (Kou et al., 1993; Pope & Fry, 1997), made

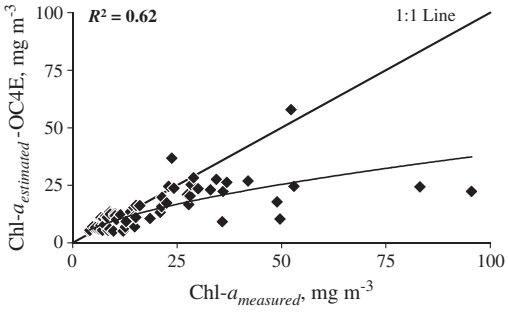

Fig. 5. Chl-*a* concentrations estimated by the MERIS OC4E algorithm plotted versus analytically measured chl-*a* concentrations.

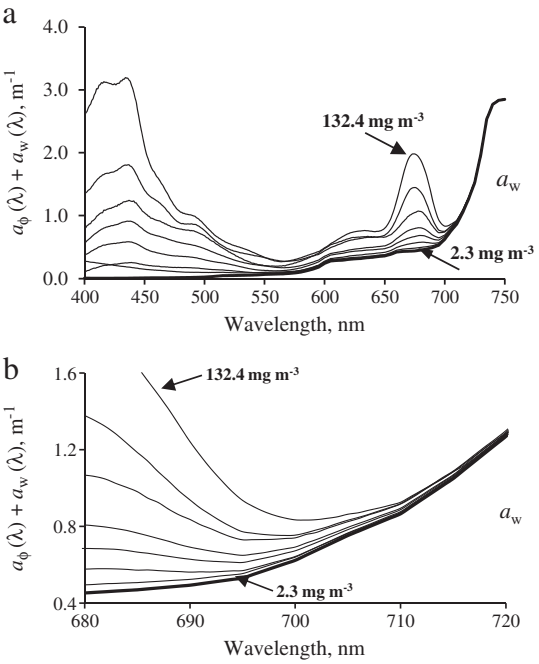

Fig. 6. Spectra of the combined absorption coefficients of phytoplankton and water for chl-*a* concentrations from 2.3 to 132.4 mg m^{-3} (a), and the position of the minimal combined absorption by chl-*a* and water in the red region (b). The thick line represents the absorption coefficient of water (Mueller, 2003).

the red region suitable for the development of algorithms for the remote estimation of chl-*a* concentrations in inland and coastal waters.

Many of these algorithms relied on the magnitude of the reflectance peak around 700 nm. With an increase in chl-*a* concentration, the magnitude of the absorption peak at 675 nm and its width increase and the point of the minimal combined absorption by phytoplankton pigments and water, responsible for the reflectance peak around 700 nm, shifts (Fig. 6) toward longer wavelengths (Gitelson, 1992; Vasilkov & Kopelevich, 1982). The shift in the position of the reflectance peak is apparent for the Fremont Lakes 2008 dataset, where it shifted from 688 nm for a chl-*a* concentration of 9.8 mg m^{-3} to 704 nm for a chl-*a* concentration of 81.2 mg m^{-3}.

3.4. NIR-red models for estimating chl-a concentrations

The FLH, firstly applied for the remote estimation of chl-*a* concentrations by Neville and Gower (1977), showed a very weak relationship with chl-*a* concentration for the Fremont Lakes 2008 dataset ($R^2 = 0.22$). Gitelson (1992) studied the shift in the position of the reflectance peak around 700 nm toward longer wavelengths with an increase in chl-*a* concentration and suggested to use the reflectance line

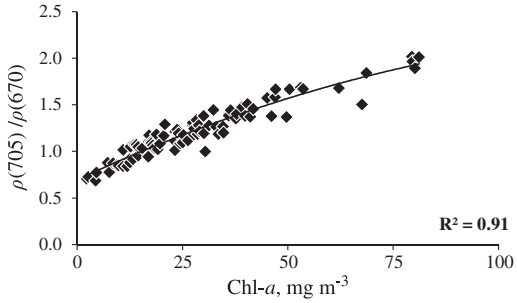

Fig. 7. Relationship of $\rho(705)/\rho(670)$ and chl-*a* concentration.

height (RLH), the magnitude of the reflectance peak above a baseline from 675 to 730 nm, instead of the FLH. Even though the values were still widely scattered around the regression line, the relationship of RLH versus chl-*a* concentration was reasonable ($R^2 = 0.48$), when the RLH was applied to the Fremont Lakes 2008 dataset, and improved significantly ($R^2 = 0.82$), when the RLH was normalized to the reflectance minimum around 675 nm (Gitelson, 1992). Simpler models, like the two band model $\rho(705)/\rho(670)$, where $\rho(705)$ is close to the average position of the reflectance peak in the NIR region and $\rho(670)$ is the reflectance close to the chl-*a* absorption maximum, estimated chl-*a* concentrations very accurately and the relationship of $\rho(705)/\rho(670)$ vs. chl-*a* concentration was very close ($R^2 = 0.91$, Fig. 7). This model (Eq. 5) has been applied successfully in many studies since it was devised in 1985 (Gitelson et al., 1985).

The optimal spectral regions for the three-band model (Eq. 3) and the two-band model (Eq. 5) were identified for the Fremont Lakes 2008 dataset through minimal values of the standard error of the estimate (STE) for linear regressions between the measured chl-*a* concentrations and model values (Dall'Olmo & Gitelson, 2005). The optimal wavelengths for the three-band model (Eq. 3) were $\lambda_1 = 666$ nm, $\lambda_2 = 712$ nm, and $\lambda_3 = 724$ nm and the optimal wavelengths for the two-band model (Eq. 5) were $\lambda_1 = 666$ nm and $\lambda_2 = 713$ nm.

3.5. Model calibration

Relationships between chl-*a* concentrations and model values were established for the dataset taken in 2008. The three-band model (Eq. 3) and the two-band model (Eq. 5) were calibrated within the spectral bands of MERIS, and the two-band model (Eq. 4) was calibrated within the spectral bands of MODIS. λ_1 was set to MERIS band 7 (660–670 nm) and MODIS band 13 (662–672 nm) and λ_2 for the three-band model (Eq. 3) and two-band model (Eq. 5) was set to MERIS band 9 (703.75–713.75 nm). The optimal λ_3 for the three-band model (Eq. 3) and two-band model (Eq. 4) coincided with one of the atmospheric absorption bands of water vapor (Grossmann & Browell, 1989) and is, therefore, inapplicable for the estimation of chl-*a* concentrations with satellite sensors. The STE for the identification of the optimal λ_3 increased only slightly when λ_3 was set to MERIS band 10 (750.0–757.5 nm) for the three-band model (Eq. 3) and MODIS band 15 (743–753 nm) for the two-band model (Eq. 4):

$$\text{MERIS three} - \text{band model} = \left[\rho_{rs}^{-1}(\text{band 7}) - \rho_{rs}^{-1}(\text{band 9})\right] \times \rho_{rs}(\text{band 10}) \quad (9)$$

$$\text{MERIS two} - \text{band model} = \rho_{rs}^{-1}(\text{band 7}) \times \rho_{rs}(\text{band 9}) \quad (10)$$

$$\text{MODIS two} - \text{band model} = \rho_{rs}^{-1}(\text{band 13}) \times \rho_{rs}(\text{band 15}). \quad (11)$$

For chl-*a* concentrations ranging from 0 to 100 mg m^{-3}, the MERIS three-band model (Eq. 9) and MERIS two-band model (Eq. 10) showed very close relationships ($R^2 = 0.95$) with chl-*a* concentration, which differed only slightly from linear relationships (Fig. 8). There was a reasonable linear relationship ($R^2 = 0.75$) between chl-*a* concentrations and the MODIS two-band model (Eq. 11), though the spread of the points from the best fit function is apparent for stations with low-to-moderate chl-*a* concentrations, from 0 to 25 mg m^{-3}, where the reliability of this model was very low. The algorithms for the remote estimation of chl-*a* concentrations, identified through the calibration of the models, were:

$$\text{Chl}-a = 315.50 \times (\text{MERIS 3BM})^2 + 215.95 \times (\text{MERIS 3BM}) + 25.66 \quad (12)$$

for the MERIS three-band model (Eq. 9)

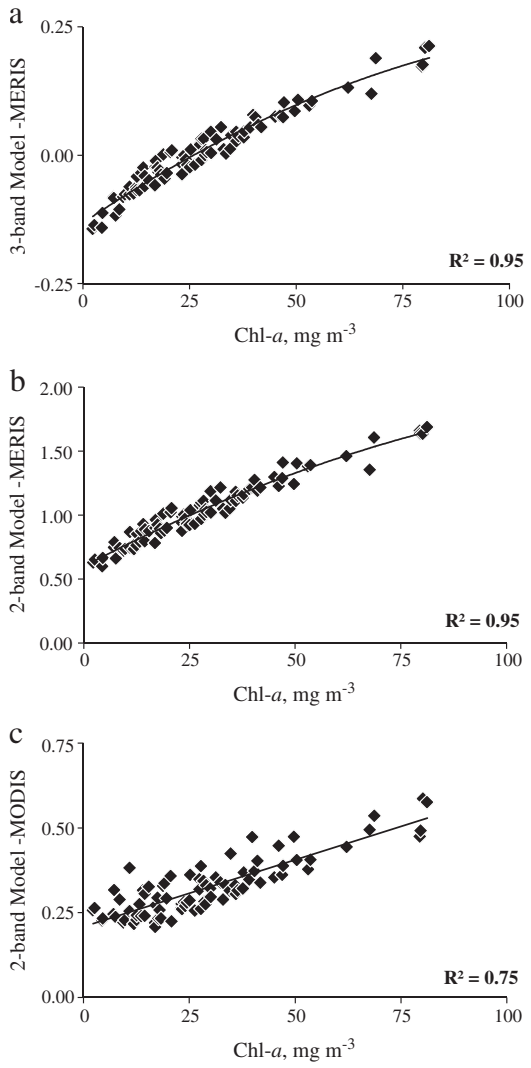

Fig. 8. Calibration of the MERIS three-band model Eq. (9) (a), MERIS two-band model Eq. (10) (b) and MODIS two-band model Eq. (11) (c) for the estimation of chl-*a* concentrations from 0 to 100 mg m^{-3} (Fremont Lakes 2008 dataset).

$$\text{Chl}-a = 25.28 \times (\text{MERIS 2BM})^2 + 14.85 \times (\text{MERIS 2BM}) - 15.18 \quad (13)$$

for the MERIS two-band model (Eq. 10) and

$$\text{Chl}-a = 190.34 \times (\text{MODIS 2BM}) - 32.45 \quad (14)$$

for the MODIS two-band model (Eq. 11).

3.6. Model validation

The independent and statistically significantly different dataset collected in 2009 was used for the validation of the models. Firstly, the reflectances measured in 2009 were simulated in the spectral bands of MERIS and MODIS and themodel values were calculated by Eqs. (9)–(11). Secondly, the chl-*a* concentrations were estimated by Eqs. (12)–(14). Finally, the estimated chl-a concentrations, chl-$a_{\text{estimated}}$, were compared with the observed chl-*a* concentrations, chl-a_{observed}.

3.6.1. MERIS three-band algorithm, two-band algorithm and enhanced three-band index

For chl-*a* concentrations from 0 to 100 mg m^{-3}, the results of the validation (Fig. 9a and c, Table 3) of the MERIS three-band and two-band algorithms (Eqs. 12 and 13) were practically identical. The difference in the MAE was small and statistically insignificant (Student's *t*-test, $p = 0.63$). For chl-*a* concentrations in the range from 0 to 25 mg m^{-3}, the difference in the MAE was statistically significant (Student's *t*-test, $p < 0.01$). The MERIS two-band algorithm was more accurate than the MERIS three-band algorithm, with an MAE of 1.2 mg m^{-3} compared to 1.9 mg m^{-3} for the MERIS three-band algorithm and an MNAE of 11.5% compared to 21.5% for the MERIS three-band algorithm (Fig. 9b and d, Table 4).

The difference in the performance of these algorithms for the estimation of chl-*a* concentrations from 0 to 25 mg m^{-3} is probably related to the use of the reflectance at λ_3 in the MERIS three-band model. $\rho(\lambda_3)$ is practically insensitive to absorption by pigments, NAP, and CDOM, but is susceptible to scattering by suspended particles and is, consequently, highly correlated with TSS ($r_s = 0.65$, $p < 0.01$) and the particulate backscattering coefficient at λ_3 ($r_s = 0.87$ for ρ_{rs}(band 10) vs. b_{bp} (740), $p < 0.01$). For chl-*a* concentrations from 0 to 25 mg m^{-3}, the correlation between $b_{bp}(\lambda)$ and TSS concentrations increased consistently toward longer wavelengths — from $r_s = 0.69$ at 570 nm to $r_s = 0.72$ at 660 nm and $r_s = 0.75$ at 740. This indicates an increased effect of the particle concentration on $b_b(\lambda)$ with an increase in wavelength and, thereby, invalidates the assumption of spectral independence of $b_b(\lambda)$ in the wavelength range from λ_1 through λ_3 for the three-band model (Dall'Olmo et al., 2003). Thus, the effects of $b_b(\lambda)$ might not be fully removed using $\rho(\lambda_3)$ and could introduce uncertainties in the estimation of chl-*a* concentrations if the MERIS three band model is applied. Especially for chl-*a* concentrations from 0 to 25 mg m^{-3}, where the reflectance is highly affected by scattering by suspended particles, differences in the sensitivity of $b_b(\lambda)$ to suspended particles could cause significant changes in the output of the MERIS three-band model. Therefore, even though the model was calibrated for a wide range of biophysical and optical water quality parameters, with ISS concentrations from 0.1 to 5.8 g m^{-3} and OSS concentrations from 0.8 to 12.8 g m^{-3}, some caution is advised if the MERIS three-band algorithm (Eq. 12), derived for the Fremont Lakes, is applied to waters with different ranges of ISS and OSS concentrations.

Recently, Yang et al. (2010) modified the three-band model and introduced the enhanced three-band index in the form:

$$\left[\text{Chl}-a\right] \propto \left[\rho_{rs}^{-1}(\lambda_1) - \rho_{rs}^{-1}(\lambda_2)\right] \times \left[\rho_{rs}^{-1}(\lambda_3) - \rho_{rs}^{-1}(\lambda_2)\right]^{-1} \quad (15)$$

where the term $\rho_{rs}(\lambda_3)$ was replaced by $[\rho_{rs}^{-1}(\lambda_3) - \rho_{rs}^{-1}(\lambda_2)]^{-1}$ to compensate for absorption and scattering by suspended particles at λ_3 in highly turbid waters. We validated the relationship between chl-*a* concentrations and the enhanced three-band index, established for chl-*a* concentrations from 30 to 120 mg m^{-3} at Lake Kasumigure, Japan, for the spectral bands of MERIS (Yang et al., 2010), using the Fremont Lakes 2009 dataset. Its accuracy was comparable to the MERIS three-band algorithm, and similarly, it was much less accurate than the MERIS two-band algorithm for the estimation of low-to-moderate chl-*a* concentrations (Tables 3 and 4).

3.6.2. MODIS two-band algorithm

The MODIS two-band algorithm (Eq. 14) was much less accurate than the MERIS three-band algorithm (Eq. 12), the MERIS two-band algorithm (Eq. 13), and the enhanced three-band index (Eq. 15) for the estimation of chl-*a* concentrations (Fig. 10a and b), which was especially pronounced for chl-*a* concentrations from 0 to 25 mg m^{-3}, where the MAE was 3.1 mg m^{-3} and the MNAE was 30.9% (Table 4). These results are expected. Stumpf and Tyler (1988) were well aware of the limitations related to the use of spectral bands in the red and NIR regions and suggested to apply the model for the estimation of moderate to high chl-*a* concentrations typical for phytoplankton blooms.

3.6.3. Comparison with Gons' algorithm

We investigated the performance of Gons' model (Eq. 2) with simulated bands 7, 9 and 12 of the MERIS standard product (Gons et al.,

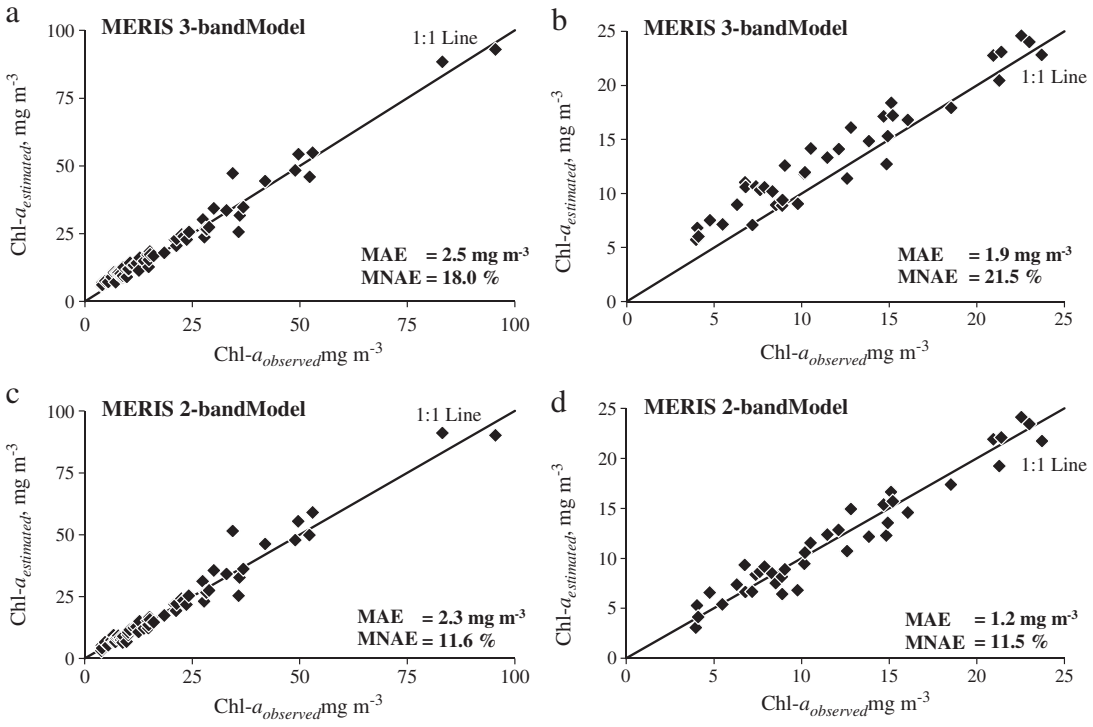

Fig. 9. Application of the MERIS three-band model (a, b) and MERIS two-band model (c, d), calibrated for the Fremont Lakes (2008 dataset) for the estimation of chl-*a* in the Fremont Lakes (2009 dataset). The plots on the right correspond to low-to-moderate chl-*a* concentrations from 0 to 25 mg m^{-3}.

2005). This model is only slightly different from the MERIS two-band model (Eqs. 5 and 10) and if the MERIS two-band model is reformulated in terms of $a(\lambda)$ and $b_b(\lambda)$, it is possible to derive Gons' model, assuming the effects of $a_{NAP}(\lambda)$ and $a_{CDOM}(\lambda)$ are insignificant compared to the effects of $a_\varphi(\lambda)$ and $a_w(\lambda)$ in the relevant spectral regions, and b_b is wavelength independent. We found a slightly non-linear relationship between the estimated and measured chl-*a* concentrations. The applied algorithm significantly underestimated chl-*a* concentrations with an MAE of 5.9 mg m^{-3} for chl-*a* concentrations from 0 to 100 mg m^{-3} and an MAE of 3.1 mg m^{-3} for chl-*a* concentrations from 0 to 25 mg m^{-3} (Tables 3 and 4). We, therefore, re-parameterized the algorithm for the Fremont Lakes 2008 dataset. The coefficients for $a^*_\varphi(665)$ and p were found through minimizing the STE. The identified $a^*_\varphi(665)$ of 0.0115 m^{-1} differed only slightly from the average $a^*_\varphi(665)$ of 0.0120 m^{-1} for the Fremont Lakes 2008 dataset. The exponent p was set to 1.024. When we applied the re-parameterized algorithm for the Fremont Lakes 2009 dataset, the MAE was 2.3 mg m^{-3} for chl-*a* concentrations from 0 to 100 mg m^{-3} and 1.4 mg m^{-3} for chl-*a* concentrations from 0 to 25 mg m^{-3} and the results were practically identical to the results for the MERIS two-band algorithm. The difference between the results from Gons' algorithm and the MERIS two-band algorithm seemed mainly caused by the difference in $a^*_\varphi(665)$, whereas the re-parameterization of p seemed to have only a limited effect on the relationship between the measured and estimated chl-*a* concentrations. The algorithm was only slightly affected by variations in b_b and 99.2% of its variability were explained by $\rho(\text{band } 7)^{-1} \times \rho(\text{band } 9)$, i.e. the two-band model (Eq. 10). These findings indicate a high potential for a simpler two-band NIR-red algorithm, without the retrieval of b_b from the NIR wavelengths, to accurately estimate chl-*a* concentrations in turbid productive waters.

3.6.4. Advanced MERIS three-band and two-band algorithms

Gilerson et al. (2010) studied comprehensive synthetic datasets of reflectance spectra and inherent optical properties, combined with the Fremont Lakes 2008 dataset, to evaluate the sensitivities of the MERIS three-band and two-band models (Eqs. 9 and 10) and the MODIS two-band model (Eq. 11) to changes in the optical water quality parameters. In contrast to the MERIS three-band and MERIS two-band models, which were mainly controlled by terms related to $a_w(\lambda)$ and $a^*_\varphi(\lambda)$ and relatively insensitive to $a_{CDOM}(\lambda)$ and $b_b(\lambda)$, the MODIS two-band model was very sensitive to changes in the optical water quality parameters and was found inapplicable for the estimation of low-to-moderate chl-*a* concentrations. Gilerson et al. (2010) reformulated the MERIS three-band and two-band models in terms of $a(\lambda)$ and $b_b(\lambda)$ and

Table 3
Performance of the NIR-red algorithms for the estimation of chl-*a* concentrations from 0 to 100 mg m^{-3}.

Model		MAE mg m^{-3}	RMSE mg m^{-3}	MNAE %
MERIS three-band algorithm	Eq. (12)	2.5	3.3	18.0
MERIS two-band algorithm	Eq. (13)	2.3	3.6	11.6
MODIS two-band algorithm	Eq. (14)	4.6	6.1	27.6
Enhanced three-band index	Eq. (15)	3.0	4.0	18.5
Gons' algorithm		5.9	8.6	26.7
Advanced MERIS three-band algorithm	Eq. (19)	3.4	5.8	15.6
Advanced MERIS two-band algorithm	Eq. (20)	2.8	5.0	12.6

MAE — *m*ean *a*bsolute *e*rror, RMSE — *r*oot *m*ean *s*quared *e*rror, and MNAE — *m*ean *n*ormalized *a*bsolute *e*rror.

Table 4
Performance of the NIR-red algorithms for the estimation of chl-*a* concentrations from 0 to 25 mg m^{-3}.

Model		MAE mg m^{-3}	RMSE mg m^{-3}	MNAE %
MERIS three-band algorithm	Eq. (12)	1.9	2.1	21.5
MERIS two-band algorithm	Eq. (13)	1.2	1.4	11.5
MODIS two-band algorithm	Eq. (14)	3.1	3.8	30.9
Enhanced three-band index	Eq. (15)	2.5	2.9	22.4
Gons' algorithm		3.1	3.5	26.6
Advanced MERIS three-band algorithm	Eq. (19)	1.4	1.6	15.2
Advanced MERIS two-band algorithm	Eq. (20)	1.2	1.6	11.9

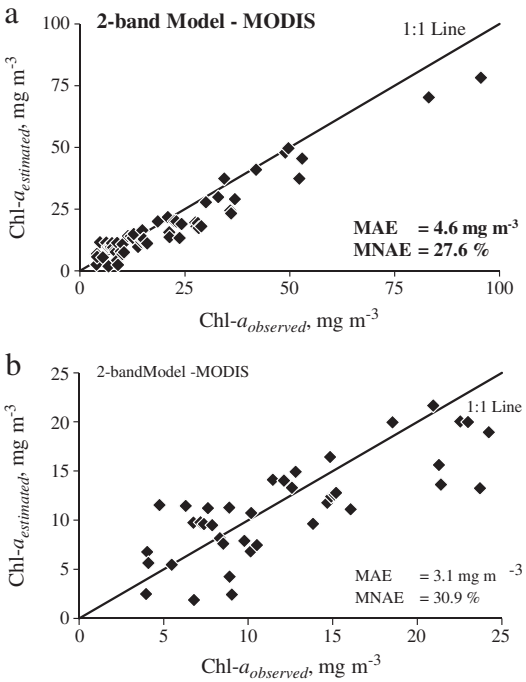

Fig. 10. Application of the MODIS two-band model, calibrated for the Fremont Lakes (2008 dataset), for the estimation of chl-*a* in the Fremont Lakes (2009 dataset).

separated $a(\lambda)$ into $a_{\varphi}(\lambda)$, $a_{NAP}(\lambda)$, $a_{CDOM}(\lambda)$, and $a_w(\lambda)$, to develop simplified semi-analytical models for the remote estimation of chl-*a* concentrations, which were slightly different from Gons' model (Eq. 2):
Advanced MERIS three-band model

$$\text{Chl}-a = \frac{[\text{MERIS 3 BM}(a_w(754)) - a_w(708) + a_w(665)]}{a^*_{\varphi}(665)} \quad (16)$$

Advanced MERIS two-band model

$$\text{Chl}-a = \frac{[\text{MERIS 2 BM}(a_w(708)) - a_w(665)]}{a^*_{\varphi}(665)} \quad (17)$$

where MERIS 3BM and MERIS 2BM are the model values derived from Eqs. (9) and (10), respectively, using ρ_{rs}(band 7), ρ_{rs}(band 9), and ρ_{rs}(band 10). The substitution of $a^*_{\varphi}(665)$ with a value derived from the synthetic and field datasets and of $a_w(\lambda)$ with values from the literature resulted in the final algorithms:
Advanced MERIS three-band algorithm

$$\text{Chl}-a = (113.36 \times \text{MERIS 3 BM} + 16.45)^{1.124} \quad (18)$$

Advanced MERIS two-band algorithm

$$\text{Chl}-a = (35.75 \times \text{MERIS 2BM} - 19.30)^{1.124}. \quad (19)$$

The algorithms (Eqs. 18 and 19) were applied to estimate chl-*a* concentrations for the Fremont Lakes 2009 dataset. The advanced MERIS three-band algorithm estimated chl-*a* concentrations in the Fremont Lakes accurately with an MAE of 3.4 mg m^{-3} and an MNAE of 15.6% for chl-*a* concentrations from 0 to 100 mg m^{-3} (Table 3). The algorithm worked very accurately for chl-*a* concentrations from 0 to 25 mg m^{-3} with an MAE of 1.4 mg m^{-3} and an MNAE of 15.2% (Table 4). The results for the estimation of chl-*a* concentrations from 0 to 25 mg m^{-3} were only slightly different from those of the MERIS two-band model and the advanced MERIS two-band algorithm (Tables 3 and 4).

3.6.5. Statistical comparison of the NIR-red models

To compare the accuracy of the models an ANOVA, followed by Tukey's HSD multiple comparison procedure was performed. Tukey's HSD indicated statistically significant differences, when the absolute estimation errors from the MERIS two-band algorithm (Eq. 13), the algorithm with the smallest MAE for chl-*a* concentrations from 0 to 100 mg m^{-3} and 0 to 25 mg m^{-3}, were compared to the errors from the MODIS two-band algorithm (Eq. 14) and Gons' algorithm (Gons et al., 2005) for chl-*a* concentrations from 0 to 100 mg m^{-3} ($p<0.05$). Differences were more pronounced for chl-*a* concentrations from 0 to 25 mg m^{-3}, where Tukey's HSD indicated statistically significant differences, when the errors from the MERIS two-band algorithm (Eq. 13) were compared to the errors from the MERIS three-band algorithm (Eq. 12), the MODIS two-band algorithm (Eq. 14), the MERIS enhanced three-band index (Eq. 15), and Gons' algorithm. The MERIS two-band algorithm (Eq. 13), the re-parameterized Gons' algorithm, the advanced MERIS three-band algorithm (Eq. 18), and the advanced MERIS two-band algorithm (Eq. 19) successfully estimated chl-*a* concentrations from 0 to 25 mg m^{-3} with MAEs from 1.2 to 1.4 mg m^{-3} and MNAEs from 11.5 to 15.2% (Table 4). These results indicate a high potential of the simple MERIS two-band model for the reliable estimation of chl-*a* concentrations in inland and coastal waters with low-to-moderate chl-*a* concentrations, without any reduction in accuracy compared to the more complex models, even though more research seems required to analyze the sensitivity of the model to differences in $a^*_{\varphi}(665)$. Interestingly enough, Yacobi et al. (2011), studying the performances of the two- and three-band models using reflectance spectra taken at Lake Kinneret, estimated chl-*a* concentrations very accurately with a linear algorithm only slightly different from Eq. 13.

4. Conclusions

This study presented a detailed description of the bio-physical and bio-optical water quality parameters measured in the Fremont Lakes, Nebraska, which were comparable to water quality parameters typical for inland and coastal waters around the world. The effects of the presence of NAP and CDOM, which make the algorithms typically applied for oceanic waters inapplicable for optically complex inland and coastal waters, were presented for lakes with a wide range of chl-*a* and TSS concentrations. The importance of the red and NIR spectral regions for the development of algorithms for the remote estimation of chl-*a* concentrations in inland and coastal waters was shown.

Several NIR-red models for the remote estimation of chl-*a* concentrations were evaluated and the rationale behind these models was presented. The MERIS three-band model estimated chl-*a* concentrations with an MAE of 2.5 mg m^{-3} for chl-*a* concentrations from 0 to 100 mg^{-3} and with an MAE of 1.9 mg m^{-3} for chl-*a* concentrations from 0 to 25 mg m^{-3}. The MERIS two-band model, estimated chl-*a* concentrations with an MAE of 2.3 mg m^{-3} for chl-*a* concentrations from 0 to 100 mg m^{-3} and with an MAE of 1.2 mg m^{-3} for chl-*a* concentrations from 0 to 25 mg m^{-3}. These models, and the advanced MERIS models were the most accurate in chl-*a* estimation.

This study showed the accurate estimation of chl-*a* concentrations by several models using the spectral bands of MERIS, where the simplest model, the MERIS two-band model, provided the most accurate estimation of chl-*a* concentrations below 25 mg m^{-3}, and has a high potential for the development of a simple universally applicable NIR-red algorithm.

Acknowledgments

We would like to thank D.-C. Rundquist from CALMIT at the University of Nebraska - Lincoln for his support at the different stages of this study. B. Leavitt provided technical support in the field. We are indebted to T. Barrow from the Aquatic Ecology and Limnology

Laboratory at the University of Nebraska-Lincoln for his assistance in the field and laboratory. Y. Peng provided support in the collection of field data and laboratory work. This work was supported partially by NASA LCLUC program grant NNG06GG17G.

References

Baban, S. -M. -J. (1996). Trophic classification and ecosystem checking of lakes using remotely sensed information. *Hydrological Sciences Journal*, *41*, 939–957.

Babin, M., Morel, A., & Gentili, B. (1996). Remote sensing of sea surface sun-induced chlorophyll fluorescence: Consequences of natural variations in the optical characteristics of phytoplankton and the quantum yield of chlorophyll a fluorescence. *International Journal of Remote Sensing*, *17*, 2417–2448.

Babin, M., Stramski, D., Ferrari, G. -M., Claustre, H., Bricaud, A., Obolensky, G., et al. (2003). Variations in the light absorption coefficients of phytoplankton, nonalgal particles, and dissolved organic matter in coastal waters around Europe. *Journal of Geophysical Research*, *108*, 3211–3230.

Bidigare, R. -R., Ondrusek, M. -E., Morrow, J. -H., & Kiefer, D. -A. (1990). In-vivo absorption properties of algal pigments. *Proceedings of SPIE*, *1302*, 290–302.

Binding, C. -E., Jerome, J. -H., Bukata, R. -P., & Booty, W. -G. (2008). Spectral absorption properties of dissolved and particulate matter in Lake Erie. *Remote Sensing of Environment*, *112*, 1702–1711.

Bricaud, A., Babin, M., Morel, A., & Claustre, H. (1995). Variability in the chlorophyll-specific absorption coefficients of natural phytoplankton: Analysis and parameterization. *Journal of Geophysical Research*, *100*, 13321–13332.

Bricaud, A., Morel, A., & Prieur, L. (1981). Absorption by dissolved organic matter of the sea (yellow substance) in the UV and visible domains. *Limnology and Oceanography*, *26*, 43–53.

Carder, K. -L., Steward, R. -G., Harvey, G. -R., & Ortner, P. -B. (1989). Marine humic and fulvic acids: Their effects on remote sensing of ocean chlorophyll. *Limnology and Oceanography*, *34*, 68–81.

Carlson, R. -E. (1977). A trophic state index for lakes. *Limnology and Oceanography*, *22*, 361–369.

Cleveland, J. -S., & Weidemann, A. -D. (1993). Quantifying absorption by aquatic particles: A multiple scattering correction for glass-fiber filters. *Limnology and Oceanography*, *38*, 1321–1327.

Costanza, R., d'Arge, R., de Groot, R., Farber, S., Grasso, M., Hannon, B., et al. (1997). The value of the world's ecosystem services and natural capital. *Nature*, *387*, 253–260.

Dall'Olmo, G. (2006). Isolation of optical signatures of phytoplankton pigments in turbid productive waters: remote assessment of chlorophyll-a. PhD dissertation, University of Nebraska-Lincoln, Lincoln, NE.

Dall'Olmo, G., & Gitelson, A. -A. (2005). Effect of bio-optical parameter variability on the remote estimation of chlorophyll-a concentration in turbid productive waters: Experimental results. *Applied Optics*, *44*, 412–422.

Dall'Olmo, G., Gitelson, A. -A., & Rundquist, D. -C. (2003). Towards a unified approach for the remote estimation of chlorophyll-a in both terrestrial vegetation and turbid productive waters. *Geophysical Research Letters*, *30*, 4 1938.

Dekker, A.-G. (1993). Detection of optical water quality parameters for eutrophic waters by high resolution remote sensing. Doctoral thesis, Vrije Universiteit, Amsterdam.

Dekker, A. -G., Malthus, T. -J., & Seyhan, E. (1991). Quantitative modeling of inland water quality for high resolution systems. *IEEE Transactions on Geoscience and Remote Sensing*, *29*, 89–95.

Eaton, A. -D., Clesceri, L. -S., Rice, E. -W., Greenberg, A. -E., & Franson, M. -A. -H. (Eds.). (2005). *Standard methods for the examination of water and wastewater: Centennial edition*. Baltimore, MD: American Public Health Association United Book Press, Inc., (Sections 2540 D. Total suspended solids dried at 103–105 °C and 2540 E. Fixed and volatile solids ignited at 550 °C.).

Ferrari, G. -M., & Tassan, S. (1999). A method using chemical oxidation to remove light absorption by phytoplankton pigments. *Journal of Phycology*, *35*, 1090–1098.

Gilerson, A., Gitelson, A. -A., Zhou, J., Gurlin, D., Moses, W. -J., Ioannou, I., et al. (2010). Algorithms for remote estimation of chlorophyll-a in coastal and inland waters using red and near infrared bands. *Optics Express*, *18*, 24109–24125.

Gitelson, A. (1992). The peak near 700 nm on radiance spectra of algae and water: relationships of its magnitude and position with chlorophyll concentration. *International Journal of Remote Sensing*, *13*, 3367–3373.

Gitelson, A. -A., Dall'Olmo, G., Moses, W., Rundquist, D., Barrow, T., Fisher, T. -R., et al. (2008). A simple semi-analytical model for remote estimation of chlorophyll-a in turbid productive waters: Validation. *Remote Sensing of Environment*, *112*, 3582–3593.

Gitelson, A. -A., Gritz, Y., & Merzlyak, M. -N. (2003). Relationships between leaf chlorophyll content and spectral reflectance and models for non-destructive chlorophyll assessment in higher plant leaves. *Journal of Plant Physiology*, *160*, 271–282.

Gitelson, A. -A., Gurlin, D., Moses, W., & Yacobi, Y. (2011). Remote estimation of chlorophyll-*a* concentration in inland, estuarine, and coastal waters. In Q. Weng (Ed.), *Advances in environmental remote sensing: sensors, models, and applications* (pp. 449–478). Boca Raton: CRC Press, Taylor and Francis Group.

Gitelson, A., Keydan, G., & Shishkin, V. (1985). Inland waters quality assessment from satellite data in visible range of the spectrum. *Sovjet Journal of Remote Sensing*, *6*, 28–36.

Gitelson, A. -A., & Kondratyev, K. -Y. (1991). Mechanism producing the near-700 nm brightness peak in the emission spectra of water bodies and its possible applications in remote sounding of such bodies. *Transactions of the U.S.S.R. Academy of Sciences: Earth Science Sections*, *306*, 1–4.

Gitelson, A. -A., Nikanorov, A. -M., Szabo, G. -Y., & Szilagyi, F. (1986). Etude de la qualité des eaux de surface par télédétéction. *Monitoring to detect changes in water quality series (Proceedings of the Budapest Symposium, July 1986), IAHS Publ. no. 157* (pp. 111–121).

Gons, H. -J. (1999). Optical teledetection of chlorophyll a in turbid inland waters. *Environmental Science & Technology*, *33*, 1127–1132.

Gons, H. -J., Auer, M. -T., & Effler, S. -W. (2008). MERIS satellite chlorophyll mapping of oligotrophic and eutrophic waters in the Laurentian Great Lakes. *Remote Sensing of Environment*, *112*, 4098–4106.

Gons, H. -J., Rijkeboer, M., Bagheri, S., & Ruddick, K. -G. (2000). Optical teledetection of chlorophyll a in estuarine and coastal waters. *Environmental Science & Technology*, *34*, 5189–5192.

Gons, H. -J., Rijkeboer, M., & Ruddick, K. -G. (2002). A chlorophyll-retrieval model for satellite imagery (Medium Resolution Imaging Spectrometer) of inland and coastal waters. *Journal of Plankton Research*, *24*, 947–951.

Gons, H. -J., Rijkeboer, M., & Ruddick, K. -G. (2005). Effect of a waveband shift on chlorophyll retrieval from MERIS imagery of inland and coastal waters. *Journal of Plankton Research*, *27*, 125–127.

Gordon, H. -R. (1973). Simple calculation of the diffuse reflectance of the ocean. *Applied Optics*, *12*, 2803–2804.

Gordon, H. -R., Brown, O. -B., & Jacobs, M. -M. (1975). Computed relationships between the inherent and apparent optical properties of a flat homogeneous ocean. *Applied Optics*, *14*, 417–427.

Gordon, H. -R., & Morel, A. -Y. (1983). Remote assessment of ocean color for interpretation of satellite visible imagery — A review. In R. -T. Barber, C. -N. -K. Mooers, M. -J. Bowman, & B. Zeitzschel (Eds.), *Lecture notes on coastal and estuarine studies 4*. New York: Springer Verlag.

Gower, J. -F. -R. (1980). Observations of in situ fluorescence of chlorophyll-a in Saanich inlet. *Boundary-Layer Meteorology*, *18*, 235–245.

Gower, J. -F. -R., Doerffer, R., & Borstad, G. -A. (1999). Interpretation of the 685 nm peak in water-leaving radiance spectra in terms of fluorescence, absorption and scattering, and its observation by MERIS. *Int. J. Remote Sens., 20*, 1771–1786.

Gower, J., & King, S. (2007). Validation of chlorophyll fluorescence derived from MERIS on the west coast of Canada. *International Journal of Remote Sensing*, *28*, 625–635.

Grossmann, B. -E., & Browell, E. -V. (1989). Spectroscopy of water vapour in the 720 nm wavelength region: Line strengths, self-induced pressure broadenings and shifts, and temperature dependence of linewidths and shifts. *Journal of Molecular Spectroscopy*, *136*, 262–294.

Han, L., & Rundquist, D. -C. (1997). Comparison of NIR/RED ratio and first derivative of reflectance in estimating algal-chlorophyll concentration: A case study in a turbid reservoir. *Remote Sensing of Environment*, *62*, 253–261.

Hayase, K., & Tsubota, H. (1985). Sedimentary humic acid and fulvic acid as fluorescent organic materials. *Geochimica et Cosmochimica Acta*, *49*, 159–163.

Kallio, K., Kutser, T., Hannonen, T., Koponen, S., Pulliainen, J., Vepsäläinen, J., et al. (2001). Retrieval of water quality parameters of various lake types in different seasons. *Science of the Total Environment*, *268*, 59–77.

Koponen, S., Attila, J., Pulliainen, J., Kallio, K., Pyhälahti, T., Lindfors, A., et al. (2007). A case study of airborne and satellite remote sensing of a spring bloom event in the Gulf of Finland. *Continental Shelf Research*, *27*, 228–244.

Koponen, S., Pulliainen, J., Kallio, K., & Hallikainen, M. (2002). Lake water clarity classification with airborne hyperspectral spectrometer and simulated MERIS data. *Remote Sensing of Environment*, *79*, 51–59.

Kou, L., Labrie, D., & Chylek, P. (1993). Refractive index of water and ice in the 0.65-to 2.5-μm spectral range. *Applied Optics*, *32*, 3531–3540.

Kutser, T., Hiire, M., Metsamaa, L., Vahtmäe, E., Paavel, B., & Aps, R. (2009). Field measurements of spectral backscattering coefficient of the Baltic Sea and boreal lakes. *Boreal Environment Research*, *14*, 305–312.

Lillesand, T. -M., Johnson, W. -L., Deuell, R. -L., Lindstorm, O. -M., & Meisner, D. -E. (1983). Use of Landsat data to predict the trophic state of Minnesota Lakes. *Photogrammetric Engineering and Remote Sensing*, *49*, 219–229.

Mitchell, B. -G., Kahru, M., Wieland, J., & Stramska, M. (2003). Determination of spectral absorption coefficients of particles, dissolved material and phytoplankton for discrete water samples. In J. -L. Mueller, G. -S. Fargion, & C. -R. McClain (Eds.), *Inherent optical properties: Instruments, characterizations, field measurements and data analysis protocols. Ocean Optics Protocols for Satellite Ocean Color Sensor Validation, revision 4, IV*, Goddard Space Flight Center Technical Memorandum 2003-211621.

Mittenzwey, K. -H., Breitwieser, S., Penig, J., Gitelson, A. -A., Dubovitzkii, G., Garbusov, G., et al. (1991). Fluorescence and reflectance for the in-situ determination of some quality parameters of surface waters. *Acta Hydrochimica et Hydrobiologica*, *19*, 3–15.

Mittenzwey, K. -H., Ullrich, S., Gitelson, A. -A., & Kondratiev, K. -Y. (1992). Determination of chlorophyll a of inland waters on the basis of spectral reflectance. *Limnology and Oceanography*, *37*, 147–149.

Morel, A., & Gentili, B. (1991). Diffuse reflectance of oceanic waters: its dependence on Sun angle as influenced by the molecular scattering contribution. *Applied Optics*, *30*, 4427–4438.

Morel, A., & Gentili, B. (1993). Diffuse reflectance of oceanic waters. II. Bidirectional aspects. *Applied Optics*, *32*, 6864–6879.

Morel, A., & Prieur, L. (1977). Analysis of variations in ocean color. *Limnology and Oceanography*, *22*, 709–722.

Moses, W. -J., Gitelson, A. -A., Berdnikov, S., & Povazhnyy, V. (2009). Satellite estimation of chlorophyll-a concentration using the red and NIR Bands of MERIS — The Azov Sea case study. *IEEE Geoscience and Remote Sensing Letters*, *6*, 845–849.

Mueller, J.-L. (2003). Inherent optical properties: instrument characterizations, field measurements and data analysis protocols. In: Ocean Optics Protocols for Satellite Ocean Color Sensor Validation, Revision 4, Volume IV, Erratum 1 to Pegau, S., Zanefeld,

J.-R.-V. & Mueller, J.-L. (2003) Inherent optical property measurement concepts: physical principles and instruments. In: J.-L. Mueller, G.-S. Fargion, & C.-R. McClain (Eds.) *Inherent optical properties: Instruments, characterizations, field measurements and data analysis protocols*. Ocean Optics Protocols for Satellite Ocean Color Sensor Validation, revision 4, volume IV, Goddard Space Flight Center Technical Memorandum 2003-211621.

Neville, R. -A., & Gower, J. -F. -R. (1977). Passive remote sensing of phytoplankton via chlorophyll a fluorescence. *Journal of Geophysical Research*, *82*, 3487–3493.

Nusch, E. -A. (1980). Comparison of different methods for chlorophyll and phaeopigment determination. *Archiv für Hydrobiologie–Beiheft Ergebnisse der Limnologie*, *14*, 14–36.

O'Reilly, J. -E., Maritorena, S., O'Brien, M. -C., Siegel, D. -A., Toole, D., Menzies, D., et al. (2000). In S. -B. Hooker, & E. -R. Firestone (Eds.), *SeaWiFS postlaunch calibration and validation analyses. SeaWiFS postlaunch technical report series*, *11, (3)*, NASA Technical Memorandum 2000-206892, Volume 11.

Ohde, T., & Siegel, H. (2003). Derivation of immersion factors for the hyperspectral TriOS radiance sensor. *Journal of Optics A — Pure and Applied Optics*, *5*, L12–L14.

Pegau, W. -S., Gray, D., & Zaneveld, J. -R. V. (1997). Absorption and attenuation of visible and near-infrared light in water: Dependence on temperature and salinity. *Applied Optics*, *36*, 6035–6046.

Pope, R. -M., & Fry, E. -S. (1997). Absorption spectrum (380–700 nm) of pure water. II. Integrating cavity measurements. *Applied Optics*, *36*, 8710–8723.

Quibell, G. (1991). The effect of suspended sediment on reflectance from freshwater algae. *International Journal of Remote Sensing*, *12*, 177–182.

Ritchie, R. -J. (2008). Universal chlorophyll equations for estimating chlorophylls a, b, c, and d and total chlorophylls in natural assemblages of photosynthetic organisms using acetone, methanol, or ethanol solvents. *Photosynthetica*, *46*, 115–126.

Ryan, J. -P., Fischer, A. -M., Kudela, R. -M., Gower, J. -F. -R., King, S. -A., Marin, R., III, et al. (2009). Influences of upwelling and downwelling winds on red tide bloom dynamics in Monterey Bay, California. *Continental Shelf Research*, *29*, 785–795.

Strömbeck, N., & Pierson, D. -C. (2001). The effects of variability in the inherent optical properties on estimations of chlorophyll a by remote sensing in Swedish reservoirs. *Science of the Total Environment*, *268*, 123–137.

Stumpf, R. -P., & Tyler, M. -A. (1988). Satellite detection of bloom and pigment distributions in estuaries. *Remote Sensing of Environment*, *24*, 385–404.

Thiemann, S., & Kaufmann, H. (2002). Lake water quality monitoring using hyperspectral airborne data — A semi-empirical multisensory and multitemporal and multispectral approach for the Mecklenburg Lake District, Germany. *Remote Sensing of Environment*, *81*, 228–237.

Vasilkov, A., & Kopelevich, O. (1982). Reasons for the appearance of the maximum near 700 nm in the radiance spectrum emitted by the ocean layer. *Oceanology*, *22*, 697–701.

Welschmeyer, N. -A. (1994). Fluorometric analysis of chlorophyll *a* in the presence of chlorophyll *b* and phaeopigments. *Limnology and Oceanography*, *39*, 1985–1992.

WET Labs, Inc.. (2008). *ECO 3-measurement sensor (triplet) user's guide. (revision O)*. Philomath: WET Labs, Inc.

Yacobi, Y. -Z., Moses, W. -J., Kaganovsky, S., Sulimani, B., Leavitt, B. -C., & Gitelson, A. -A. (2011). NIR-red reflectance-based models for chlorophyll-a estimation in mesotrophic inland and coastal waters: Lake Kinneret case study. *Water Research*, *45*, 2428–2436.

Yang, W., Matsushita, B., Chen, J., Fukushima, T., & Ma, R. (2010). An enhanced three-band index for estimating chlorophyll-a in turbid case-II waters: Case studies of Lake Kasumigaura, Japan, and Lake Dianchi, China. *IEEE Geoscience and Remote Sensing Letters*, *7*, 655–659.